# The ACCM Beamlines for Bioscience Studies

*To meet the increasing demand of X-ray beamlines for bioscience studies, a superconducting wiggler (SW6) was installed at TLS in 2004 and three beamlines were built using the wiggler X-ray source. A double crystal monochromator (DCM) beamline (BL13B) takes the central beam for MAD/SAD experiments on high-throughput protein structure determination. Two side-branch beamlines, BL13A and BL13C, employ asymmetric-cut curved crystal monochromator (ACCM) for fixed energy experiments: BL13C for crystal screening, drug design, and high-resolution structural study, and BL13A for scattering experiments on biomaterials such as membranes. The monochromators of both beamlines are capable of energy scanning from 12 keV to 14 keV. The newly designed ACCMs offer good performance in terms of flux, resolution, and stability, and are now ready for users.*

A total of 13 mrad horizontal radiation fan is available from the SW6 source and is shared by three beamlines. The arrangement of optics has been optimized to fully utilize the radiation fan, as shown by the layout in Fig. 1. The central 2 mrad of the radiation fan is collected by the DCM beamline and each of the two side-branch beamlines collects 1 mrad of radiation fan in the horizontal direction. BL13A is located at 3 mrad and BL13C at 4 mrad away from the center line of the radiation fan of the source. Each ACCM beamline uses a Rh-coated, Si-substrate mirror for vertical focusing, followed by the Si(111) ACCM. The water-cooled Rh mirror is placed upstream of the ACCM to simplify the energy tuning mechanism and to reduce the heat load of the crystal by cutting off the photon beams at energies above 15 keV. Following the Rh-coated mirror, the photon beam is deflected sideways by the Si(111) ACCM and passes underneath the photon beam of the central beamline to the sample position. The ACCM also serves as the horizontal focusing element and in this way the number of optical elements is minimized. The asymmetric-cut crystal is employed to maintain the Bragg angle and good focusing property and to optimize the overall performance. The crystal and the bender mechanism are mounted on a goniometer assembly (Kohzu) that allows proper alignment of the crystal and tuning of the diffraction angles for energies from 12 keV to 14 keV, as shown in Fig. 2. The adjustable degrees of freedom include, from top to bottom, x-axis (transverse to beam), two κ's, z-axis, and θ.

The ACCM plays a critical role in determining the ultimate performance of a side-branch beamline, as it has to maintain good energy resolution and focusing properties while sustaining high heat load. The design of ACCM needs to combine efficient cooling and bending mechanisms in a compact unit that allows precision adjustment on a goniometer assembly. To achieve this goal, our ACCM features a specially designed piezo-driven bender that minimizes the center displacement during bending, and employs a larger cooling area either directly under the beam footprint, or from

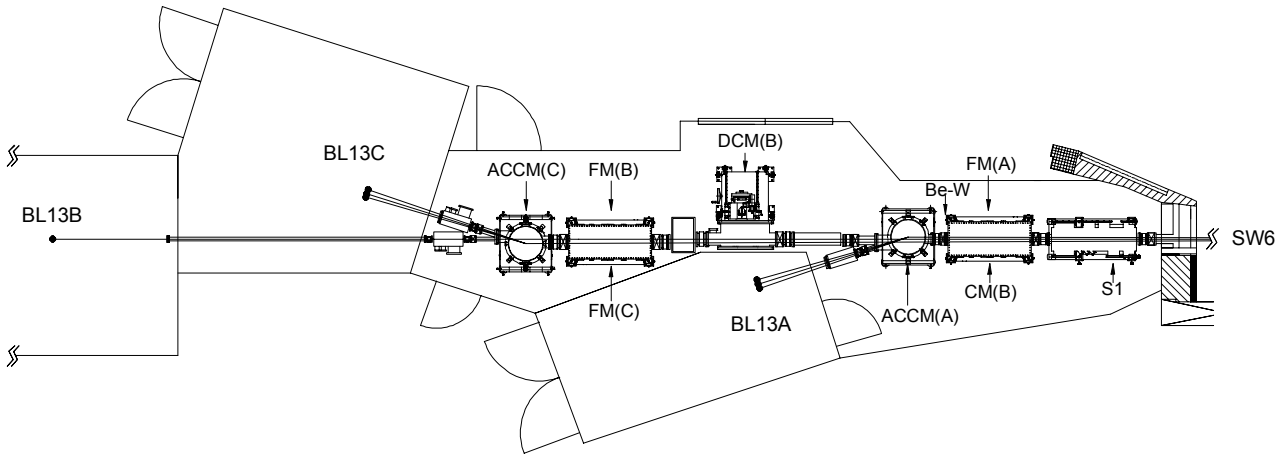


*Fig. 1: Layout of the SW6 beamlines BL13A, B, and C.*

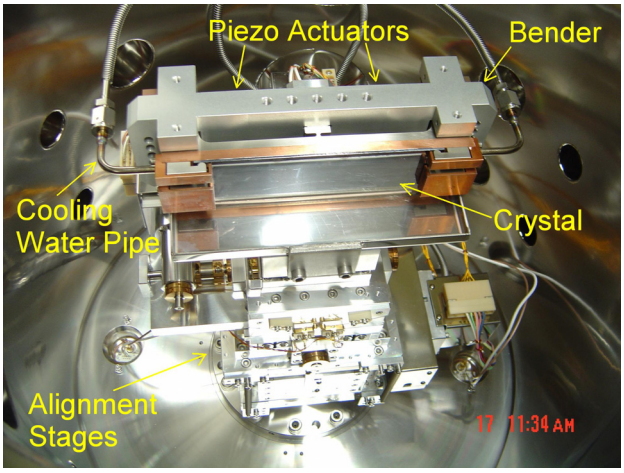


*Fig. 2: The ACCM(BL13A) viewed from the top.*

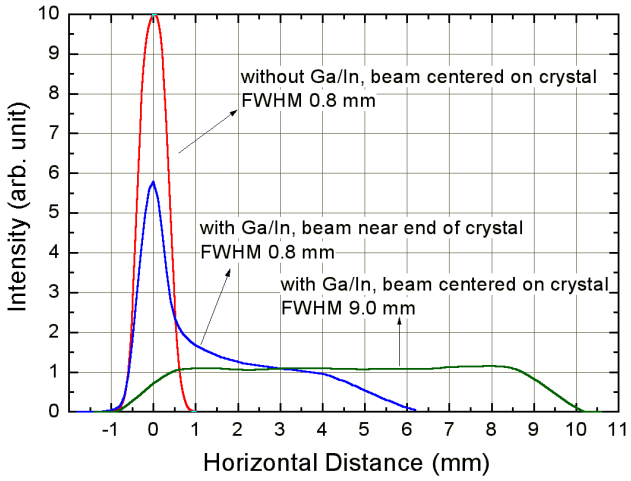


*Fig. 3: Horizontal beam profiles at focal point from ACCMs using different cooling methods.*

both sides of the crystal clamping area for more efficient heat transfer. Basically, the design uses a 2 mm thick silicon single crystal plate mounted and suspended by clamping at its two ends on a water-cooled copper block, which is brazed to a stainless steel bending structure driven symmetrically by two piezo actuators. The stainless steel structure adds rigidity and prevents twisting of the bender, and provides the necessary elasticity during bending. The structure also functions as the mounting base, and its resistance to deform with temperature change enhances the stability of the whole bender. The gap between the silicon plate and the copper block is 300 μm and is either left empty or filled with Ga/In eutectic. The Ga/In eutectic was added to improve the thermal conductivity and hence the cooling efficiency, however, this thin layer of Ga/In exerts a great amount of attractive force to the crystal surface, deforms the crystal shape, and lowers the performance of the monochromator in certain areas, as will be discussed in the following para-graphs.

Performance of the beamline is examined by measuring the diffracted and focused X-ray beams with either a pair of gas cells or a 2θ goniometer assembly. The former consists of two identical gas cells of 5 cm length in tandem that use air as the ionization medium. A 100 μm selenium or lead thin film are placed in between the two gas cells to measure the absorption edges to aid in photon energy calibration. The pair of gas cells in tandem is mounted on an x-y-z stage to facilitate scanning of the beam profile. The 2θ goniometer assembly is mounted downstream of the gas cells to analyze the energy content of the focused beam, with a Si(111) crystal.

The horizontal profiles of the diffracted X-ray beams from the ACCM are shown in Fig. 3. The profiles for the case with Ga/In layer were obtained when the X-ray beam footprint lies either at the central area or near one end of the crystal where it is clamped. The profile from the ACCM without the Ga/In layer was obtained from the crystal central area. For the case of using Ga/In layer, the profile from the crystal center is wide and shows low intensity; the profile from the area near crystal end shows a peak with a long tail. The profile obtained from the case without Ga/In layer has high intensity and a symmetrical line shape. The peak intensity of the case with Ga/In layer is lower than the case without Ga/In, because only part of the source is properly diffracted and focused. The full widths at half maximum (FWHM) for both peaks are comparable at 0.8 mm. The low intensity in the long tail and the nearly unfocused beam from the crystal central area of the Ga/In case result from the surface profile of the crystal that could not effectively diffract and focus all the extended wiggler source points in the horizontal plane. Although the long trace profiler (LTP) measurements for both cases show similar shape and radius, the LTP may not reveal short range surface distortions caused by the

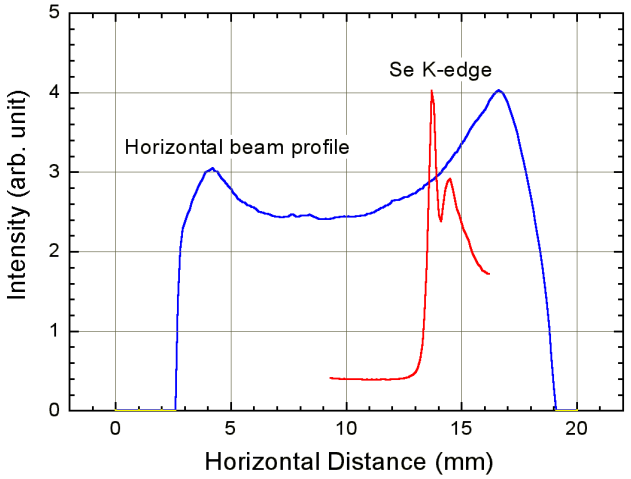


*Fig. 4: Horizontal beam profile (blue) and Se K-edge (red) obtained simultaneously by scanning a 100 μm slit with a pair of gas cells and Se film.*

Ga/In thin layer. In the Ga/In case where beam footprint is near one end of crystal, the peak in the profile originates from the area near the clamping end of the crystal, and this indicates that the crystal shape in this area is less deformed by the Ga/In layer. Although in the case with Ga/In layer the profile is less focused with lower intensity, it covers an energy range wide enough such that an absorption spectrum can be easily obtained without tuning the ACCM. This is illustrated in Fig. 4 where the Se K-edge absorption spectrum was obtained by simply scanning a 100 μm slit in the horizontal direction together with a Se film at a fixed Bragg angle. The energy position of the diffracted beam was calibrated either by the absorption edge or a 2θ-scan energy analyzer.

The vertical profiles of the diffracted X-ray beams at the focal point, from the ACCM with and without Ga/In layer, were measured by scanning the gas cell with slit opening at 20 μm, as shown in Fig. 5. Both profiles exhibit a tail characteristic of a long (80cm) cylindrical surface reflecting at a low grazing incidence angle. The profile from the case without Ga/In has higher intensity and a narrower width (FWHM 109 μm), than the case with Ga/In (FWHM 283 μm). The FWHM for the case without Ga/In is close to the calculated value of 110 μm, indicating that the bender is able to maintain stability without twisting the crystal during bending. Apparently, the thin Ga/In layer also affects the crystal shape in the sagittal direction substantially.

The photon flux from ACCM through a horizontal slit of fixed opening can be adjusted by changing the horizontal focusing condition, i.e., the crystal bending radius. However, high photon flux is always gained at the expense of energy resolution for ACCM focusing, as can be seen in Fig. 6, in which the flux and energy resolution (ΔE/E) through

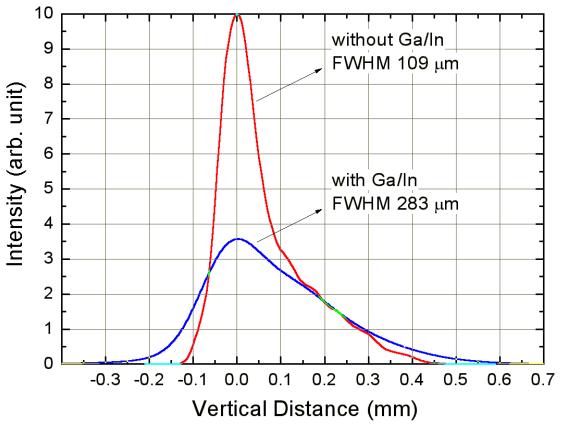


*Fig. 5: Vertical beam profiles at focal point from ACCMs using different cooling methods.*

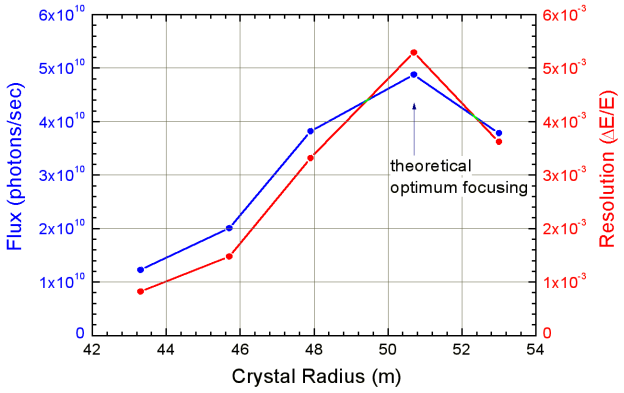


*Fig. 6: Flux and energy resolution as a function of crystal radius.*

a pair of 100 μm (H×V) slits are plotted separately against the crystal bending radius measured by LTP. The peak flux of $4.8 \times 10^{10}$ photons/sec at 50.7 m is obtained at the theoretical radius of optimum focusing, and is accompanied by the lowest resolution at $5.2 \times 10^{-3}$. At either smaller (over bending) or larger (under bending) radius, the flux decreases while the resolution increases. A similar relationship between flux and resolution can also be observed by changing the horizontal radiation source fan collected by ACCM, as shown in Fig. 7. As the source fan decreases, we gain energy resolution but with lower flux. The flux and resolution obtained from the case with Ga/In layer follow similar relationship, as indicated in the same figure with alphabetical symbols. Table 1 summarizes the flux and resolution measurements of BL13A and C for cases with and without Ga/In. With control over the source radiation fan and the crystal bending radius, various operation modes are available for users to optimize for high flux or high resolution for their specific experiments.

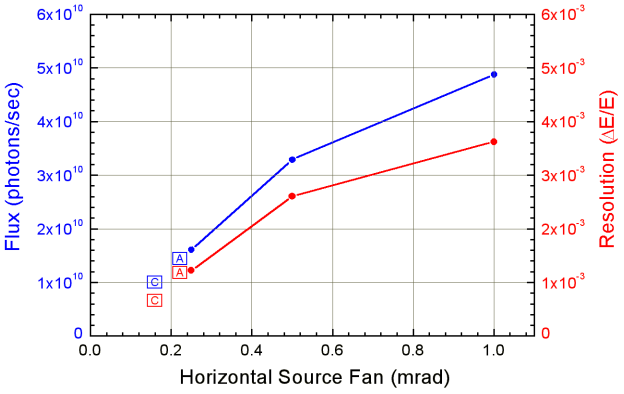


*Fig. 7: Flux and energy resolution as a function of horizontal source fan accepted by the crystal. Symbol "A" denotes data for BL13A with Ga/In, and "C" for BL13C with Ga/In.*

*Table 1: Flux and resolution of ACCM beamlines.*

| Beamline | Cooling | Energy (keV) | Slits (HxV, μm) | Flux (photons/sec) | Resolution (ΔE/E) |
|---|---|---|---|---|---|
| 13A | w/o Ga/In | 12.7 | 100×100 | $4.9 \times 10^{10}$ | $5.3 \times 10^{-3}$ |
| | Ga/In | 12.7 | 100×100 | $1.4 \times 10^{10}$ | $1.2 \times 10^{-3}$ |
| | | | 200×200 | $4.6 \times 10^{10}$ | $1.9 \times 10^{-3}$ |
| | | | 300×300 | $8.7 \times 10^{10}$ | $2.2 \times 10^{-3}$ |
| 13C | Ga/In | 12.7 | 100×100 | $1.0 \times 10^{10}$ | $6.6 \times 10^{-4}$ |
| | | | 200×200 | $3.1 \times 10^{10}$ | $8.1 \times 10^{-4}$ |
| | | | 300×300 | $5.3 \times 10^{10}$ | $9.3 \times 10^{-4}$ |
| | Ga/In | 13.5 | 100×100 | $4.5 \times 10^{9}$ | $2.3 \times 10^{-4}$ |
| | | | 200×200 | $1.6 \times 10^{10}$ | $5.4 \times 10^{-4}$ |
| | | | 300×300 | $3.0 \times 10^{10}$ | $7.8 \times 10^{-4}$ |

The cooling efficiency has been tested by turning off and on the high intensity X-ray beam on the crystal. For the case of cooling with Ga/In, the result is excellent and shows no significant change in performance at storage ring current of 200 mA. For the case without Ga/In layer, the performance of ACCM shows slight change during the first few minutes after the crystal is exposed to the X-ray beam from the 200 mA stored current. A better cooling mechanism is thus required for operation under higher stored ring current. Using a Ga/In layer thicker than 500 μm might be a good choice since it will reduce the influence of the layer to the crystal shape.

As shown by the above measurements, the newly designed ACCM offers good performances in terms of flux, resolution, and stability. The cooling design could be further improved for enhanced stability when operated with higher storage ring current. At present, both SW6 side-branch beamlines BL13A and BL13C are well-equipped with this ACCM and are ready for users' research in bioscience.

**BEAMLINE**
13A1 X-ray Scattering beamline
13C1 Protein Crystallography beamline

**AUTHORS**
C.-I Ma, S.-H. Chang, C.-Y. Liu, J.-M. Juang, C.-H. Chang, and K.-L. Tsang
National Synchrotron Radiation Research Center, Hsinchu, Taiwan

**PUBLICATIONS**

- C. H. Chang, C. I. Ma, L. J. Huang, J. Y. Yuh, and K. L. Tsang, NSRRC Activity Report, 96(2003/2004).
- C. I. Ma, C. H. Chang, L. J. Huang, C. C. Chen, P. C. Tseng, H. S. Fung, S. C. Chung, S. Y. Perng, D. J. Wang, Y. C. Jean, K. L. Tsang, and C.-T. Chen, Proc. of the 8th Int'l Conf. on Synchrotron Radiation Instrumentation, **705**, 687 (2004).

**CONTACT E-MAIL**
cima@nsrrc.org.tw